Design and Control of a Planar Haptic Device with Passive Actuators Based on Passive Force Manipulability Ellipsoid (FME) Analysis

· · · · · · · · · · · · · · · ·   · · · · · · · · · · · · · ·

Changhyun Cho
Department of Mechanical Engineering
Korea University
Intelligent Robotics Research Center at KIST
39-1, Hawolgok-dong, Sungbuk-gu
Seoul 136-791, Republic of Korea
e-mail: chcho@kist.re.kr

Jae-Bok Song*
Department of Mechanical Engineering
Korea University
5, Anam-dong, Sungbuk-gu
Seoul 136-701, Republic of Korea
e-mail: jbsong@korea.ac.kr

Munsang Kim
Intelligent Robotics Research Center at KIST
39-1, Hawolgok-dong, Sungbuk-gu
Seoul 136-791, Republic of Korea
e-mail: munsang@kist.re.kr

In this paper, we propose an optimal design for a passive haptic device with brakes and its control method. The inability of a brake to generate torque significantly affects the performance of a multi-DOF haptic device, in that a desired force can be generated only approximately in some workspace and, in some cases, the device may become stuck contrary to the user's intention. In this research, these limitations are analyzed by means of the so-called passive force manipulability ellipsoid. Through the analysis, performance indices are developed for evaluating the limitations associated with passive haptic devices. Optimization is conducted for a 5-bar mechanism with redundant actuation, and

*To whom all correspondence should be addressed.

a coercive force approximation scheme is developed to avoid unsmooth motion during the wall-following task along the virtual wall. It is experimentally shown that the performance in relation to the limitations is greatly improved for the optimized mechanism. © 2005 Wiley Periodicals, Inc.

1. INTRODUCTION

Passive haptic devices are much more safe than active ones, because they use brakes instead of motors. However, a passive haptic device is unable to generate a force or torque in an arbitrary direction because a brake can only generate torque in the direction opposite to its motion. This inability to generate torque in other directions means that a multi-DOF passive haptic system using several brakes inevitably suffers from serious limitations. Colgate *et al.* briefly reported that a desired force can be generated only approximately in some workspace and that, contrary to the user's intention, the device may well become stuck.[1] This so-called force approximation causes unsmooth, jagged motion during the wall-following task on the virtual wall. These limitations have also been investigated with the passive FME (force manipulability ellipsoid),[2] which graphically represented the mapping between the joint space and task space of the robotic device.[3]

Colgate *et al.* proposed the unicycle-Cobot.[1] This device was designed to use the kinematic constraint of a wheel on the path guidance task (e.g., wall-following task). A version of the spatial Cobot was also presented with a special CVT (continuous variable transmission) mechanism.[4] However, the passive force display was not evaluated for the spatial Cobot. Surdilovic *et al.* presented a coupled mechanism with a differential CVT, which had features which were similar to those of the spatial Cobot, but which had a simpler design and control mechanism.[5] Book *et al.* presented a planar haptic device based on the 5-bar mechanism with four brakes providing for a 2 DOF haptic display.[6] The use of these redundant actuators greatly increases the haptic performance of the device. Trocazz *et al.* presented a PADyC (a passive arm with dynamic constraints), equipped with joint speed limiters, which was used for cardiac puncturing.[7]

Although several good passive haptic devices have been devised so far, the researchers have failed to fully explain how to analyze and deal with the above mentioned limitations, in order to improve the performance of passive haptic devices. Moreover, the lack of a proper analysis tool for passive mechanisms makes their design very complicated and time-consuming.

In this paper, we propose a passive haptic device whose performance is guaranteed. Since the limitations of passive haptic devices can be measured in the form of an angle in the passive FME,[2] we can quantitatively compute their performance, so as to obtain performance indices which are indicative of each limitation. A 5-bar mechanism with redundant actuation, as described in Ref. 6, is chosen for the optimization of the device, since it possesses several parameters which can be optimized. To avoid having an unsmooth (sometimes abrupt) force display, a coercive force approximation scheme, similar to those described,[8,9] is developed based on the passive FME analysis. The usefulness of this method of optimization and control is verified through various experiments.

This paper is organized as follows: In Section 2, the so-called passive FME analysis tool is introduced; in Section 3, the limitations of a passive haptic system are analyzed using this tool; in Section 4, performance indices indicative of the limitations are introduced; in Section 5, a redundantly actuated 5-bar mechanism is introduced, and the passive FME developed for the nonredundant mechanism is extended to the redundantly actuated mechanism; in Section 6, optimization is conducted; in Section 7, the coercive force approximation is proposed; in Section 8, experimental results are presented; finally, in Section 9, conclusions are drawn and future work is outlined.

2. PASSIVE FME ANALYSIS

In an electric brake, only the magnitude of the braking torque can be controlled, since changing the polarity of an electromagnet does not affect its direction. A brake can generate braking torque only in the passive region in which $\tau \cdot \dot{q} \leq 0$ is satisfied, where $\dot{q}$ and τ represent the joint velocity and the braking torque, respectively. Therefore, if the brake is commanded to generate a desired torque, τ_d, in the active region (i.e., $\tau_d \cdot \dot{q} > 0$), the brake control torque, τ_c, should be set to zero, since the brake cannot produce τ_d. Taking this control feature into account, the brake control torque can be computed by adopting Karnopp's stick-slip model[10] as follows:

Slip mode ($\dot{q} \neq 0$)
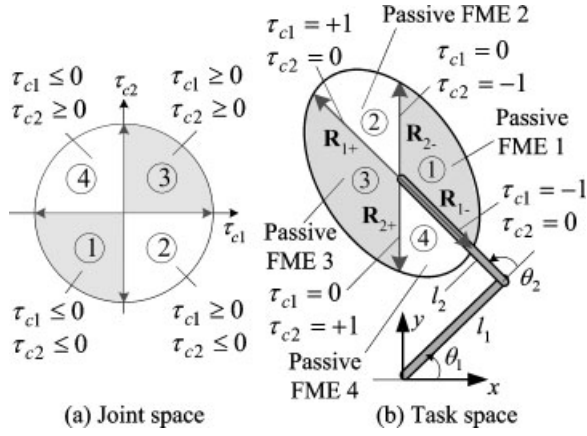
Figure 1. A set of passive FMEs ($\theta_1=45°$, $\theta_2=90°$, $l_1=l_2=l$).

$$\tau_c = \begin{cases} -\operatorname{sgn}(\dot{q})|\tau_d| & \text{if } \operatorname{sgn}(\dot{q}) \neq \operatorname{sgn}(\tau_d), \\ 0 & \text{otherwise;} \end{cases} \quad (1a)$$

Stick mode ($\dot{q}=0$)

$$\tau_c = \begin{cases} -\tau_h & \text{if } \operatorname{sgn}(\tau_h) \neq \operatorname{sgn}(\tau_d), \\ 0 & \text{otherwise,} \end{cases} \quad (1b)$$

where τ_h is the external torque acting on the brake shaft (i.e., the torque applied manually by a human operator in the case of most haptic devices). In this paper, Eq. (1) will be referred to as the *passive constraint*.

The control torques in the 2 DOF mechanism can be represented by four regions representing all possible combinations of joint velocities and hand torques, as shown in Figure 1(a). A set of passive FMEs can be drawn by mapping τ_c in joint space into the end-effector force, $\mathbf{F}_c$, in task space using Jacobian mapping [i.e., $\tau_c = \mathbf{J(q)}^T\mathbf{F}_c$]. Thus, each region in Figure 1(a) is mapped into the corresponding passive FME in Figure 1(b), which represents a set of passive FMEs. Each passive FME is delimited by four reference forces, $\mathbf{R}_{1+}$, $\mathbf{R}_{1-}$, $\mathbf{R}_{2+}$, and $\mathbf{R}_{2-}$, where $\mathbf{R}_i$ denotes the end-effector force when only brake i is applied (i.e., $\tau_{ci} \neq 0$), while the other brakes are released. For example, if $\tau_{c1} > 0$ (or $\tau_{c1} < 0$) with $\tau_{c2} = 0$, then the force $\mathbf{R}_{1+}$ (or $\mathbf{R}_{1-}$) is generated. The end-effector force, $\mathbf{F}_c$, can be obtained from the following equation:

$$\mathbf{F}_c = \mathbf{J(q)}^{-T}\tau_c. \quad (2)$$
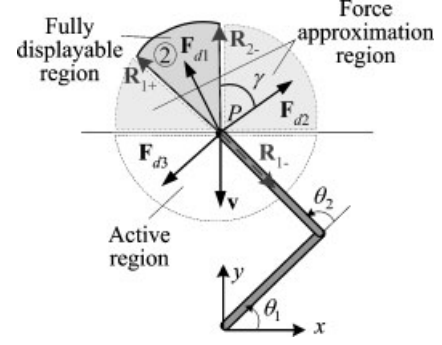
Figure 2. Force approximation ($\theta_1=45°$, $\theta_2=90°$, $l_1=l_2=l$).

For a two-link manipulator, $\mathbf{J}^{-T}$ is given by

$$\mathbf{J}^{-T} = \frac{1}{l_1 l_2 s_2}\begin{bmatrix} l_2 c_{12} & -l_1 c_1 - l_2 c_{12} \\ l_2 s_{12} & -l_1 s_1 - l_2 s_{12} \end{bmatrix} = [\mathbf{J}_1 | \mathbf{J}_2], \quad (3)$$

where $c_1 = \cos(\theta_1)$, $s_1 = \sin(\theta_1)$, $c_{12} = \cos(\theta_1 + \theta_2)$, and $s_{12} = \sin(\theta_1 + \theta_2)$. Hence, the reference forces can easily be computed by means of the following relations:

$$\mathbf{R}_{i+} = \mathbf{J}_i, \quad \mathbf{R}_{i-} = -\mathbf{J}_i, \quad (4)$$

where the subscript i denotes the joint number, and $\mathbf{J}_i$ is the ith column vector of $\mathbf{J}^{-T}$. For example, $\mathbf{R}_{1+}$ corresponds to $\tau_{c1} = 1$ and $\tau_{c2} = 0$ and, thus, $\mathbf{R}_{1+} = \mathbf{J}_1$. As the manipulator configuration changes, the Jacobian $\mathbf{J}$ and thus the reference forces vary.

3. LIMITATIONS ON PASSIVE HAPTIC DISPLAY

3.1. Force Approximation

Consider the example in Figure 2 for the purpose of conducting a detailed analysis. Suppose that the end-point, P, is moving in the $-y$ direction (i.e., $\dot{\theta}_1 < 0$ and $\dot{\theta}_2 > 0$). Hence, the brakes can generate a force only in passive FME 2 (i.e., $\tau_{c1} > 0$ and $\tau_{c2} < 0$), because of the passive constraint. The desired force, $\mathbf{F}_{d1}$, in this *fully displayable region* in Figure 2 can be displayed accurately by the resultant force of $\mathbf{R}_{1+}$ and $\mathbf{R}_{2-}$. On the other hand, the desired force, $\mathbf{F}_{d2}$, needs to be represented by the combined force of $\mathbf{R}_{2-}$ and $\mathbf{R}_{1-}$ in Figure 2. However, since the generation of $\mathbf{R}_{1-}$ requires that τ_{c1} be less than 0, which violates the passive constraint, $\tau_{c1} \cdot \dot{\theta}_1 \leq 0$, $\mathbf{F}_{d2}$ can only be displayed approximately, since it has to rely
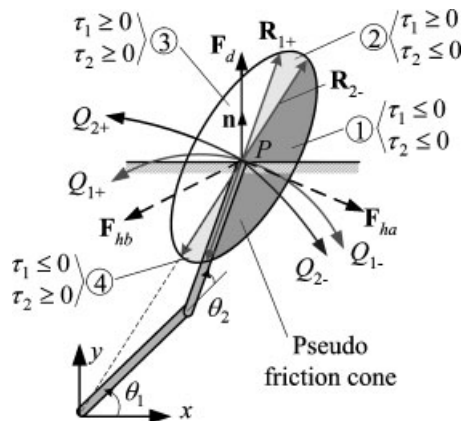
Figure 3. Example of haptic display.

on the nearest available force $\mathbf{R}_{2-}$. This region, therefore, is called a *force approximation region*, in which the desired force can be displayed only approximately. It is convenient to define a force approximation angle, γ, between $\mathbf{R}_{2-}$ and $\mathbf{F}_{d2}$, as shown in Figure 2, which represents the level of force approximation. That is, $\gamma=0$ represents the most accurate force display. Finally, the desired force, $\mathbf{F}_{d3}$, in the active region cannot be displayed at all, since it belongs to the active region of $\mathbf{F}\cdot\mathbf{v}>0$. Unlike active haptic devices, passive haptic devices possess regions in which the desired force cannot be displayed or can be displayed only approximately. These regions can easily be found using a passive FME analysis. This is why the passive FME serves as a useful tool for analyzing passive devices.

3.2. Pseudo Friction Cones

Figure 3 shows an example of a haptic display on the virtual wall, which has a unit normal vector, $\mathbf{n}$, in the direction of the y axis. For simplicity of analysis, the initial state of the passive haptic device in Figure 3 will be set in such a way that all of the joint velocities are initially zero. Because the virtual wall is assumed to have no friction, the desired force, $\mathbf{F}_d$, required to represent the virtual wall is in the same direction as $\mathbf{n}$. A force, $\mathbf{F}_h$, is assumed to be applied to the end-effector by a human operator, so that this force allows motion along the surface with which the end-effector maintains contact. $Q_{i\pm}$ in Figure 3 is one of the possible paths of the end-effector when brake i is fully activated (or locked), and "+" indicates the link rotation in the positive (i.e., counterclockwise) direction. Hence, the end-effector location

at the next instant is determined by the linear combination of Q_1 and Q_2 at the current instant. When the operator applies $\mathbf{F}_{ha}$ to move the end-effector to the right, the paths Q_{1-} and/or Q_{2-} will be induced, thus causing the end-effector to penetrate the wall. As the level of penetration increases, the brakes are more strongly activated, in order to prevent further penetration. Thus, the end-effector is likely to become stuck at the next instant. On the other hand, when the operator applies $\mathbf{F}_{hb}$ to move the end-effector to the left, the paths Q_{1+} and/or Q_{2+} will be invoked, thus leading to no penetration of the end-effector into the wall. This enables motion along the surface at the next instant.

In this example, the end-effector becomes stuck when the desired force, $\mathbf{F}_d$, is in passive FME 3 and the operator applies the force, $\mathbf{F}_{ha}$, in passive FME 1, which is located on the opposite side of passive FME 3. This example can be generalized, so that a pseudo friction cone coincides with the passive FME on the opposite side of the passive FME where the desired force exists. If the force that the operator applies by hand belongs to the pseudo friction cone, then the end-effector will become stuck, regardless of the fact that the user's intention was to move it along the surface. All four passive FMEs can belong to a pseudo friction cone, depending on the location of the desired force. The angle of the pseudo friction cone can be used as a measure of quality for the haptic display in terms of the path guidance. In other words, the smaller the angle, the better the quality.

4. PERFORMANCE INDICES

In the previous sections, the limitations of passive haptic devices were analyzed in detail. The concepts of the force approximation and the pseudo friction cone were introduced, along with the passive FME analysis tool. These quantitative analyses can be utilized in the design and control of passive haptic devices. In this section, we propose performance indices which can be used for the analysis of these limitations.

Figure 4 illustrates passive FME 1 and its corresponding velocity region (possible velocity region in Figure 4). $\mathbf{a}$ and $-\mathbf{a}$ denote the vectors normal to the end-effector velocity, $\mathbf{v}$. The force displayable region for the given velocity is delimited by $\mathbf{a}$ and $-\mathbf{a}$, and passive FME 1 exists inside this region. Since passive FME 1 does not cover the entire region, a force approximation needs to be made for the force display,
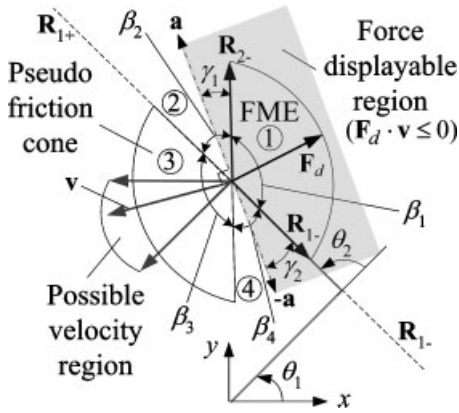
Figure 4. Approximation schematic.

when the desired force, $\mathbf{F}_d$, is located outside passive FME 1. The size of the force approximation region is given by

$$\gamma_1 + \gamma_2 = \pi - \beta_1 = \beta_2 = \beta_4, \tag{5}$$

where β_i represents the size of passive FME i. Note that the size of the force approximation region for passive FME 1 is equal to that of the nearby passive FME (in this case, β_2 or β_4). Likewise, the size of the force approximation regions for the other passive FMEs shown in Figure 1 can easily be obtained. The performance associated with the force approximation can be quantitatively measured by summing the sizes of all of the force approximation regions (i.e., the passive FMEs) for a given configuration. Since this summation is always 2π, the summation of the squared angles of the force approximation regions is used for the performance index, as in the following equation:

$$P_a = \sum_{i=1}^{n} \beta_i^2, \tag{6}$$

where n is the number of passive FMEs (in Figure 4, $n=4$). Supposing that β_i is always equal to $\pi/2$ for $i=1,\ldots,4$, for example, $P_a=\pi^2$. If $\beta_1=\beta_2=2\pi/3$ and $\beta_2=\beta_4=\pi/3$, then $P_a=10\pi^2/9$. P_a increases as the difference between the β_i's increases. Therefore, the optimization based on Eq. (6) will result in an even distribution of β_i. Since Eq. (6) represents the performance measure for a specific configuration, it is referred to as the local performance index for the force approximation. Then, the global performance index of GP_a can be defined as

$$GP_a = \frac{1}{m}\sum_{j=1}^{m} [P_a]_j = \frac{1}{m}\sum_{j=1}^{m}\left[\sum_{i=1}^{n}\beta_i^2\right]_j, \tag{7}$$

where $[P_a]_j$ denotes the local performance computed for the jth configuration, and m is the number of measurement points in the whole working volume.

As mentioned above, the pseudo friction cone coincides with the passive FME situated on the opposite side of the passive FME where the desired force is located. Because its size can be measured by the angle β_i of the passive FME, the local performance index, P_f, for the pseudo friction cone can be defined as

$$P_f = \max(\beta_1, \ldots, \beta_n). \tag{8}$$

The optimization based on Eq. (8) is considered as a min-max problem, in which the worst case (i.e., max β_i) is minimized. Thus, differences in β_i are reduced, which results in the even distribution of reference forces, as in the case of those in Eq. (6). In a similar manner to Eq. (7), the global performance index, GP_f, can be defined by

$$GP_f = \frac{1}{m}\sum_{j=1}^{m} [\max(\beta_1, \ldots, \beta_n)]_j. \tag{9}$$

5. REDUNDANTLY ACTUATED 5-BAR MECHANISM

The limitations (i.e., those associated with the force approximation and pseudo friction cone) on the haptic display using electric brakes were discussed in Section 3. Since all of the limitations associated with passive FMEs are related to the reference forces that delimit these devices, it is important to take these factors into consideration when evaluating the performance of a passive haptic device.

The main challenge in designing a passive haptic device is how to uniformly distribute the reference forces in task space. This can be achieved either by increasing the number of reference forces or by controlling the reference forces. Increasing the number of reference forces can improve the capability of the force display, but this causes the device to become unduly complicated. The use of a kinematically redundant device or a parallel mechanism with redundant actuation can allow the number of reference forces to be increased. For example, a three-link manipulator has six reference forces for the 2 DOF force display in
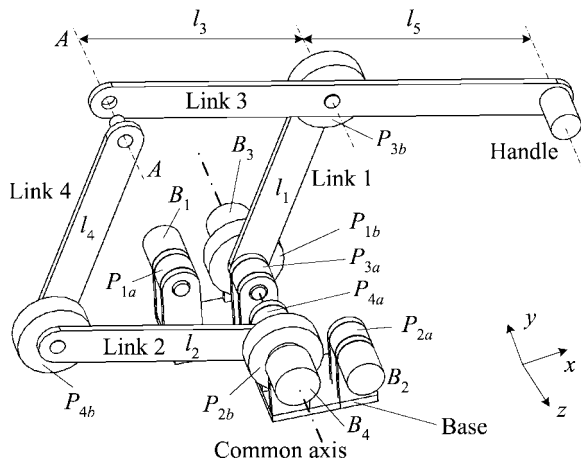
Figure 5. Redundantly actuated 5-bar mechanism and torque transmitting mechanism.

task space and, thus, this could allow broader passive FMEs to be created. In a parallel mechanism with redundant actuation,[6] the redundant DOFs of actuation can provide additional reference forces, as in the case of a kinematically redundant manipulator. On the other hand, the control of any of the parameters associated with kinematic constraints (e.g., Jacobian) would adjust the direction of the reference forces, but the design and control of such a system are usually very complicated.[4,5] Moreover, the force provided by kinematic constraints cannot be controlled. For example, suppose that a wheel rolls on the floor. The axial force of the wheel, which represents the wheel's kinematic constraint, is predetermined by the coefficient of friction, μ, and the contact force, N, unless N or μ is controlled. (In this situation, the magnitude of the axial force is μN.)

5.1. Redundantly Actuated 5-Bar Mechanism

In this research, the redundant actuation scheme is adopted to provide the 5-bar mechanism with more reference forces, as shown in Figure 5. In this figure, l_i and B_i represent the length of link i and brake i, respectively. P_i denotes the pulley of the tendon-drive system for joint i. Since four brakes are installed, the 5-bar mechanism is provided with two redundant DOFs in terms of actuation, for the 2 DOF force display in task space. To reduce the inertia of the moving parts, all of the brakes are mounted at the base. Link 1 (or link 2) rotates about the common axis located at the base, and the torque generated by brake 1 (or brake 2) can be transmitted to link 1 (or
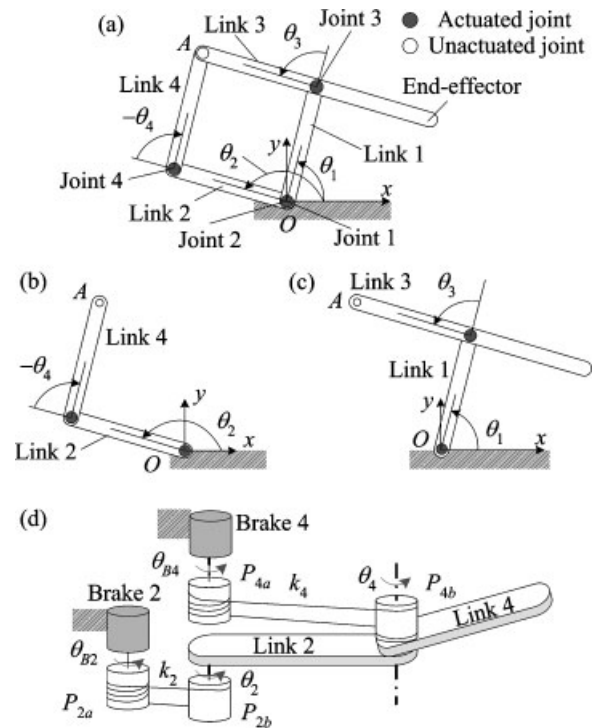
Figure 6. Example of coupled motion ($k_2 = k_4 = 1$).

link 2) directly or through a speed reducer. However, since links 3 and 4 rotate relative to links 1 and 2 (i.e., moving bodies), respectively, and brakes 3 and 4 are mounted at the base, a special torque transmitting mechanism is required to convey the torques generated by brakes 3 and 4 to the corresponding links.

A schematic of the 5-bar mechanism is provided in Figure 6(a). The 5-bar mechanism can be broken up into two two-link manipulators, as shown in Figures 6(b) and 6(c), thereby providing an easier understanding of the torque transmitting mechanism, by simplifying the mechanical structures. The detailed torque transmitting mechanism of the two-link mechanism shown in Figure 6(b) is illustrated in Figure 6(d). In Figure 6(d), θ_i and θ_{Bi} represent the joint angle and the rotating angle of the brake, respectively, and k_i is the reduction ratio of the tendon-drive system. For example, $k_4 = d_{4a}/d_{4b}$, where d_{4i} represents the diameter of P_{4i}. Brake 2 (or 4), which provides the braking torque to link 2 (or 4), is mounted at the base and conveys the torque through pulleys P_{2a} and P_{2b} (or P_{4a} and P_{4b}). In the two-link device under consideration, the brakes are connected to the links through the tendon-drive mecha-
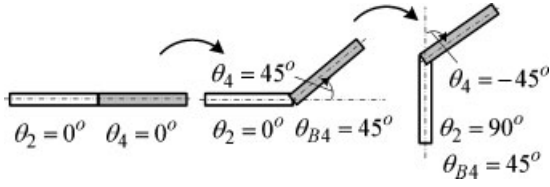
Figure 7. A 5-bar mechanism to be optimized.

nism, thus causing the joint angles to be different from the brake angles. The joint angle θ_2 is given by

$$\theta_2 = k_2 \theta_{B2} \tag{10}$$

and the joint angle θ_4 is described by

$$\theta_4 = k_4 \theta_{B4} - k_4 \theta_2. \tag{11}$$

Note that θ_4 is a function of θ_2 as well as θ_{B4}. This can be explained by considering the example in Figure 7. For example, suppose that all of the brakes are replaced by motors and all k_i's are set to 1. From the initial configuration with $\theta_2 = 0°$ and $\theta_{B4} = 0°$ (and thus $\theta_4 = 0°$), brake 4 rotates to $\theta_{B4} = 45°$ (thus $\theta_4 = 45°$) with brake 2 locked. Once it is released, brake 2 rotates to $\theta_2 = 90°$ with brake 4 being locked. The resulting configuration is described by $\theta_4 = -45°$, which can be predicted by Eq. (11). Note that the tendon can move relative to the pulley although the pulley P_{4a} is locked by brake 4. That is, a so-called coupled motion[11,12] in the wire transmission is observed in θ_4. This concept can easily be extended to the case of brakes. A similar torque transmitting mechanism to that described in Figure 6(d) is applied to the two-link mechanism shown in Figure 6(c). Therefore, the same coupled motion occurs in θ_3.

5.2. Passive FME of the Redundantly Actuated Mechanism

The 5-bar mechanism shown in Figure 5 is redundantly actuated because it generates only 2 DOF motion in the task space using four brakes. Therefore, the dependent joint angles of joints 3 and 4 can be represented by the independent joint angles of joints 1 and 2. This relation is given by

$$\dot{\Phi} = J_G \dot{\Phi}_a, \tag{12}$$

where $\dot{\Phi} = [\dot{\theta}_1 \ \dot{\theta}_2 \ \dot{\theta}_3 \ \dot{\theta}_4]^T$, $\dot{\Phi}_a = [\dot{\theta}_1 \ \dot{\theta}_2]^T$, and $J_G \in R^{4 \times 2}$ is the Jacobian matrix representing the relation between $\dot{\Phi}$ and $\dot{\Phi}_a$.[13] By the principle of virtual work, the torque relation can be obtained by

$$J_G^T \tau = \tau_a, \tag{13}$$

where $\tau = [\tau_1 \ \tau_2 \ \tau_3 \ \tau_4]^T$ and $\tau_a = [\tau_1 \ \tau_2]^T$. Since the 5-bar mechanism has 2 DOFs in the task space, the force **F** at the end-effector is given by

$$\tau_a = J^T F, \tag{14}$$

where $J \in R^{2 \times 2}$ is the Jacobian matrix of the 5-bar mechanism. Substituting Eq. (13) into (14) yields

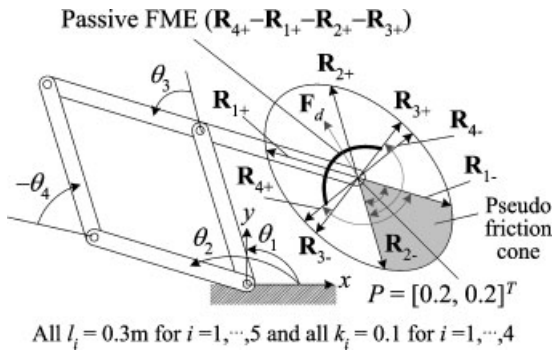$$J^{-T} J_G^T \tau = (J_r^T)^{\#} \tau = F, \tag{15}$$

where $J_r = \{(J^{-T} J_G^T)^{\#}\}^T \in R^{2 \times 4}$ is the resulting Jacobian matrix and $(\cdot)^{\#}$ represents the pseudo inverse.[13] Since $(J_r^T)^{\#} = [J_1 | J_2 | J_3 | J_4] \in R^{2 \times 4}$, eight reference forces are available, as described in Eq. (4)

$$R_{i+} = +J_i, R_{i-} = -J_i \quad (i = 1, \dots, 4). \tag{16}$$

If the angular positions and velocities for joints 1 and 2 are measured by the encoders, then those for joints 3 and 4 can also be obtained from Eq. (12). Thus, the Jacobian matrix can be computed, and the reference forces can also be obtained from Eq. (16). For example, suppose that the joint velocities are given by $\dot{\theta}_i < 0$ for all $i = 1, \dots, 4$. Referring to Eq. (1a), it is found that the braking torque $\tau_i > 0$ for all i. The reference forces can then be computed by means of the following equation:

$$R_i = +J_i \quad \text{for all } i \tag{17}$$

and therefore the passive FME $(R_{4+} - R_{1+} - R_{2+} - R_{3+})$ is generated by the given joint velocities, as shown in Figure 8. Note that this passive FME consists of three regions $R_{4+} - R_{1+}$, $R_{1+} - R_{2+}$, and $R_{2+} - R_{3+}$. Likewise, if the joint velocities are given by $\dot{\theta}_i < 0$ for $i = 1, 2, 3$ and $\dot{\theta}_4 > 0$, then the passive FME $(R_{1+} - R_{2+} - R_{3+} - R_{4-})$ is activated. That is, the passive FME of the redundantly actuated 5-bar mechanism consists of three adjacent regions. Therefore, a total of eight passive FMEs are possible in the redun-

Passive FME ($\mathbf{R}_{4+}$–$\mathbf{R}_{1+}$–$\mathbf{R}_{2+}$–$\mathbf{R}_{3+}$)

All $l_i = 0.3$m for $i = 1,\cdots,5$ and all $k_i = 0.1$ for $i = 1,\cdots,4$

Figure 8. Passive FMEs for the redundantly actuated 5-bar mechanism.

dantly actuated 5-bar mechanism, since eight regions are available, as shown in Figure 8. These are

1. $\mathbf{R}_{1+}$ – $\mathbf{R}_{2+}$ – $\mathbf{R}_{3+}$ – $\mathbf{R}_{4-}$,   2. $\mathbf{R}_{2+}$ – $\mathbf{R}_{3+}$ – $\mathbf{R}_{4-}$ – $\mathbf{R}_{1-}$,

3. $\mathbf{R}_{3+}$ – $\mathbf{R}_{4-}$ – $\mathbf{R}_{1-}$ – $\mathbf{R}_{2-}$,   4. $\mathbf{R}_{4-}$ – $\mathbf{R}_{1-}$ – $\mathbf{R}_{2-}$ – $\mathbf{R}_{3-}$,

5. $\mathbf{R}_{1-}$ – $\mathbf{R}_{2-}$ – $\mathbf{R}_{3-}$ – $\mathbf{R}_{4+}$,   6. $\mathbf{R}_{2-}$ – $\mathbf{R}_{3-}$ – $\mathbf{R}_{4+}$ – $\mathbf{R}_{1+}$,

7. $\mathbf{R}_{3-}$ – $\mathbf{R}_{4+}$ – $\mathbf{R}_{1+}$ – $\mathbf{R}_{2+}$,   8. $\mathbf{R}_{4+}$ – $\mathbf{R}_{1+}$ – $\mathbf{R}_{2+}$ – $\mathbf{R}_{3+}$.

In Section 3, the pseudo friction cone for a nonredundant mechanism was said to be determined by the passive FME situated on the opposite side of the passive FME where the desired force is located. For the redundantly actuated mechanism, however, the pseudo friction cone is determined not by the passive FME, but by the region on the opposite side of that where the desired force is located. For example, if the desired force $\mathbf{F}_d$ is placed in region $\mathbf{R}_{1+}$ – $\mathbf{R}_{2+}$ as shown in Figure 8, its pseudo friction cone is located in region $\mathbf{R}_{1-}$ – $\mathbf{R}_{2-}$.

This is easily verified by considering the nonredundant mechanism, which consists of only two brakes (e.g., brakes 1 and 2). If only brakes 1 and 2 are installed in the 5-bar mechanism, then only $\mathbf{R}_{1\pm}$ and $\mathbf{R}_{2\pm}$ are available. Therefore, the pseudo friction cone is given by region $\mathbf{R}_{1-}$ – $\mathbf{R}_{2-}$. Also, if only brakes 1 and 4 (or 2 and 3) are installed, the pseudo friction cone is given by region $\mathbf{R}_{1-}$ – $\mathbf{R}_{4+}$ (or region $\mathbf{R}_{3+}$ – $\mathbf{R}_{2-}$). From this investigation of the nonredundant mechanism, it is observed that region $\mathbf{R}_{1-}$ – $\mathbf{R}_{2-}$ is the

common region for all of the pseudo friction cones in the above case. So, if a force is input by hand in this common region, there is no way to avoid the pseudo friction cone. On the other hand, suppose that the force input by hand is located in region $\mathbf{R}_{3+}$ – $\mathbf{R}_{1-}$, which is part of region $\mathbf{R}_{3+}$ – $\mathbf{R}_{2-}$ (i.e., the pseudo friction cone for brakes 2 and 3). In this case, the pseudo friction cone can be avoided by activating brakes 1 and 4 rather than brakes 2 and 3. In this sense, therefore, only the region $\mathbf{R}_{1-}$ – $\mathbf{R}_{2-}$ can be considered to represent the pseudo friction cone, rather than the whole passive FME (i.e., $\mathbf{R}_{4-}$ – $\mathbf{R}_{1-}$ – $\mathbf{R}_{2-}$ – $\mathbf{R}_{3-}$), which is situated on the opposite side of the passive FME to which F_d belongs. Note that this extension of the passive FME to the redundantly actuated mechanism can easily be applied to that of the kinematically redundant mechanism as well.

6. OPTIMAL DESIGN OF 5-BAR MECHANISM

As discussed in the previous section, the reference forces play a key role in the performance of the passive haptic system. Since these reference forces are determined by the Jacobian mapping [i.e., Eq. (15)], it is desirable that the parameters affecting the Jacobian should be chosen for optimization in the following way:

$$\mathbf{X} = [l_1/l_5 \quad l_2/l_5 \quad l_3/l_5 \quad l_4/l_5 \quad k_3 \quad k_4]^T, \quad (18)$$

where l_i is the length of link i. Due to the design specifications, the following constraints are imposed on the link length and the reduction ratio:

$$l_{\min} \leqslant l_i \leqslant l_{\max}, \quad (19)$$

$$k_{\min} \leqslant k_i \leqslant k_{\max}. \quad (20)$$

All l_i's and k_i's were initially set to 0.3 m and 0.1, respectively.

Considering the objective functions (i.e., the two performance indices defined in Section 4) and constraints, this optimization problem can be considered as a multiobjective constrained nonlinear optimization problem. To solve a multiobjective case, the utility function method is applied, which generates a new objective function with a linear combination of given objective functions (i.e., a weighted summa-
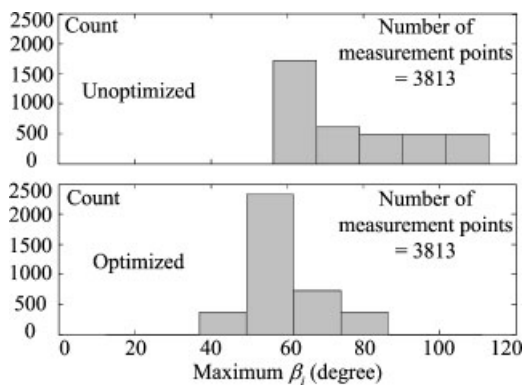
Table I. Optimization results.

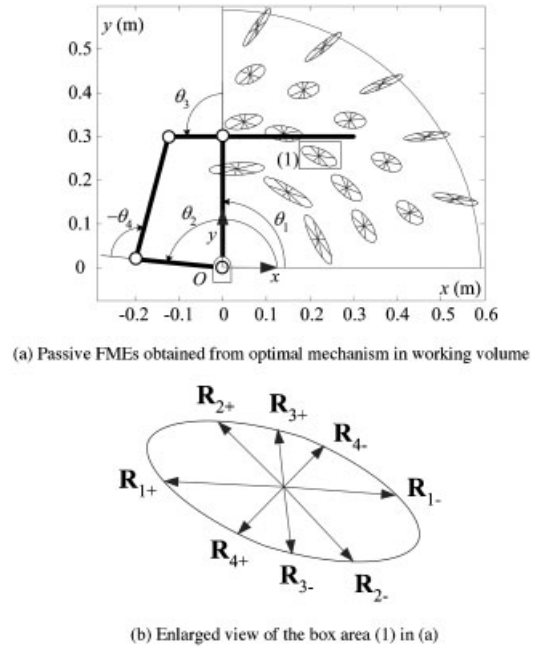|	GP$_a$	GP$_f$	Size of passive FME (β)	
			Min	Max
Before	7.509	1.614	4.0°	112.9°
After	5.310	1.035	21.1°	79.7°
		Optimal parameters		
i	1	2	3	4	5
l_i (m)	0.300	0.200	0.124	0.291	0.300
k_i			0.781	0.100	

tion). For the constrained nonlinear optimization problem, the exterior penalty function method is used along with the simplex method.[14]

The optimization results are listed in Table I and the histogram of the maximum β_i's at the measurement points is shown in Figure 9. In the unoptimized case, the maximum β_i's representing the size of the passive FME have a wide range of angles, which results in some passive FMEs being much larger in size than the others. In the optimized case, however, almost 2500 out of the 3813 measurement points have the maximum β_i's in the range between 50° and 60°. Through the histogram, we can observe that the maximum β_i's are distributed more evenly as a result of the optimization.

The passive FMEs obtained from the optimized 5-bar mechanism are illustrated in Figure 10. The passive FMEs in the working volume are shown in Figure 10(a) and a detailed view of the box area (1) in Figure 10(a) is shown in Figure 10(b). From Figure 10, we can also observe that the reference forces are rela-

(a) Passive FMEs obtained from optimal mechanism in working volume

(b) Enlarged view of the box area (1) in (a)

Figure 10. Passive FMEs obtained from optimal design.

tively evenly distributed in all directions. If the reference forces are not evenly distributed, in some cases the angles between them will be much larger than the others. In this case, the pseudo friction cones coincident with these large angles become so big that the wall-following task associated with these regions cannot be properly executed. Also, this uneven distribution may lead to a poor force approximation in some cases, since some of the angles between the reference forces are much smaller than the others, thereby leading to very small passive FME. In summary, large pseudo friction cones and poor force approximation in passive haptic devices can be avoided by optimizing them.

7. COERCIVE FORCE APPROXIMATION

The SDOF controller was proposed by Swanson and Book, in which some brakes are locked to reduce the system's DOFs.[8] This enables the execution of the wall-following task to be much smoother and can be represented as a *coercive* force approximation in the passive FME, thereby simplifying the implementation.

Suppose that the velocity of the end-effector, **v**, and the virtual wall are obtained as shown in Figure

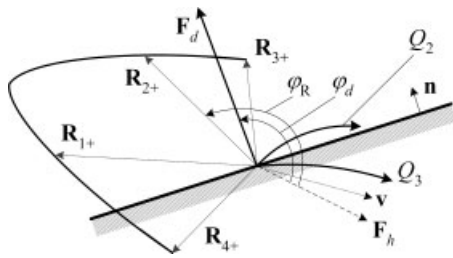**Figure 9.** Histogram of the maximum β_i's.

Figure 11. Coercive force approximation.

11. The corresponding passive FME can be drawn as shown in Figure 11, which represents part of Figure 10(b). Consider the possible paths Q_2 and Q_3. The path Q_3 causes further penetration of the end-effector into the wall, whereas Q_2 is directed out of the wall. In the SDOF controller, the path Q_2 is chosen to display the wall. That is, only brake 2 is activated for this instant. Therefore, force display is conducted with only $\mathbf{R}_{2+}$.

The force domain representation of the SDOF controller is possible without resorting to considering the possible paths. Let φ_d (or φ_R) be the angle between the hand force input, $\mathbf{F}_h$, and the desired force, $\mathbf{F}_d$ (or the reference force), in the counterclockwise direction. From the passive FME in Figure 11, the reference force $\mathbf{R}_{2+}$ used on the SDOF controller can be chosen, so that the nearest reference force satisfies $\varphi_R > \varphi_d$ during $\varphi_d \leq \pi$ (e.g., the end-effector moves to the right in Figure 11). This condition (i.e., $\varphi_R > \varphi_d$) indicates whether a possible path is directed out of the wall or not. For $\varphi_d > \pi$ (e.g., the end-effector moves to the left in Figure 8), the nearest reference force satisfying $\varphi_R < \varphi_d$ should be selected.

8. EXPERIMENTAL RESULTS

8.1. Experimental Setup

A 5-bar mechanism designed using the optimization process described in Section 6 was constructed for the experiments, as shown in Figure 12. The FT (force/torque) sensor was mounted on the handle. The rotational motion of each brake was sensed by the optical encoder mounted on the brake axis. In the experiments, brake control was conducted at a rate of 1 kHz. Since the brake was capable of generating a braking torque in proportion to the current input, it was controlled in an open-loop manner. The virtual wall was modeled in the form of a spring
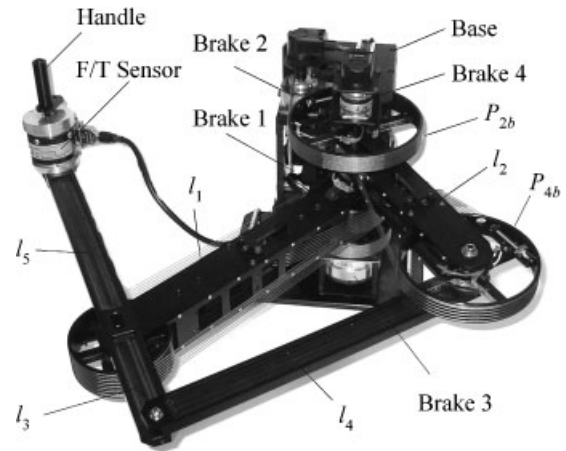

Figure 12. Experimental setup.

whose constant was 10^7 N/m, but whose surface was assumed to possess neither damping nor friction. Thus, the desired force was oriented parallel to the surface normal, $\mathbf{n}$, which coincided with the $-x$ axis, as shown in Figure 13. The virtual wall was placed at $x = 0.3$ m.

8.2. Displaying a Virtual Wall

The path of the end-effector is illustrated in Figure 13 and its detailed data are shown in Figure 14. The end-effector was moved along the $-y$ axis by the hand force, $\mathbf{F}_h$, while remaining in contact with the wall (i.e., $F_{hx} > 0$). The regions on the path marked
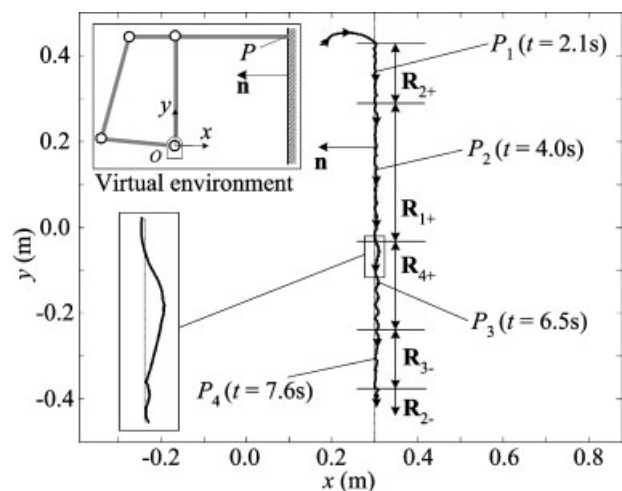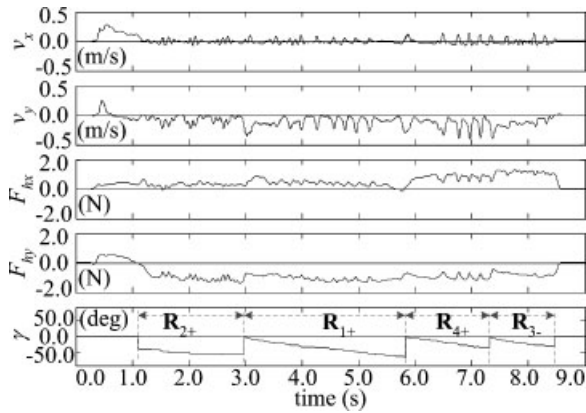

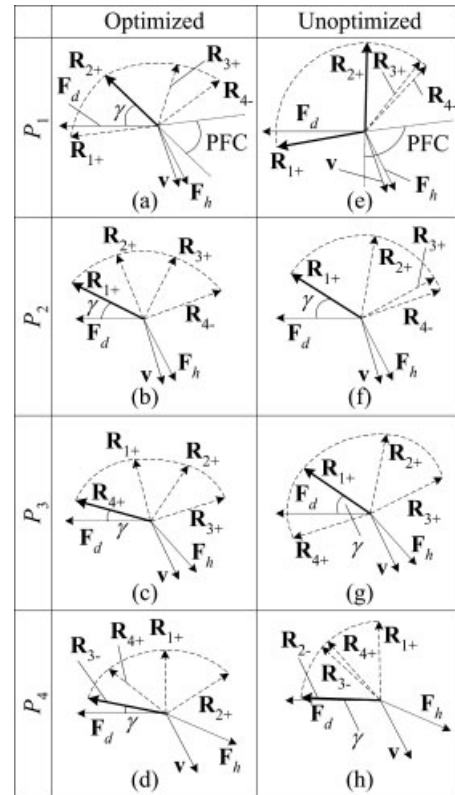**Figure 13.** Motion of the end-effector along the surface.

Figure 14. Experimental results for the display of the virtual wall.

Figure 15. Comparison of force distribution of the optimized mechanism with that of the unoptimized one.

with the reference forces in Figure 13 indicate that the force display was conducted with the corresponding reference force. For example, in the region marked with $\mathbf{R}_{1+}$, the desired force was approximately displayed with $\mathbf{R}_{1+}$. As expected, a change in the reference force tends to cause abrupt motion. The enlarged view of the box area in Figure 13 shows this type of abrupt motion.

A larger force approximation angle will produce a larger undesirable force, which significantly retards motion along the surface. That is, a large hand force input should be exerted on the end-effector to enable motion to take place along the surface, which can be observed in the plot of F_{hy}. In Figure 14, F_{hy} increases as the approximation angle γ increases. Since the angle of the force approximation is decreased by the optimization, it can be conjectured that more retarding force would be observed in the unoptimized mechanism. The maximum angle of force approximation was observed to be 65.8° during the wall-following task, just before the reference force changes from $\mathbf{R}_{1+}$ to $\mathbf{R}_{4+}$.

To describe the effectiveness of the optimization based on the proposed performance indices, the force distribution of both the optimized [(a)–(d)] and the unoptimized [(e)–(h)] 5-bar mechanisms is illustrated in Figure 15. They were computed with the same end-effector velocity, $\mathbf{v}$, and the same hand force input, $\mathbf{F}_h$, at position P_i, which is indicated in Figure 13. It should be noted that the values of v and $\mathbf{F}_h$ used for the computation were taken from the experiments with the optimized mechanism. The reference force marked with a solid line represents

that responsible for the force display in each region. For example, $\mathbf{R}_{2+}$ is used for the force approximation in Figure 15(a).

The passive FME of the unoptimized mechanism observed in Figure 15(e) shows that it can no longer move along the frictionless surface [since $\mathbf{F}_h$ exists in the pseudo friction cone (PFC)], whereas the PFC was avoided in the case of the optimized mechanism shown in Figure 15(a). However, $\|\mathbf{F}_d\|$ is almost 20 kN at time $t = 2.1$ s and this is large enough to fully lock brakes 1 and 2, so the coercive force approximation was applied in order to avoid unsmooth motion (i.e., locking of the end-effector) in the case of the optimized mechanism. The desired force $\mathbf{F}_d$ was approximately displayed by $\mathbf{R}_{2+}$, since the possible path of brake 2 is directed out of the wall (i.e., $\varphi_d > \pi$ and $\varphi_R < \varphi_d$).

Actually, the unoptimized mechanism sometimes shows better performance with respect to the force approximation, as shown in Figure 15(h). However, the evenness of distribution of the reference forces is usually poor in the case of the unopti-

mized mechanism. In most cases, except for those in Figure 15(g), $\mathbf{R}_3$ and $\mathbf{R}_4$ are closely positioned, thus leading to a large pseudo friction cone being observed, as shown in Figure 15(e). However, such a large pseudo friction cone is not observed in the case of the optimized mechanism during the wall-following task.

9. CONCLUSIONS

In this paper, we presented an optimized mechanism for a planar haptic device and its method of control. From the passive FME analysis, the limitations associated with the passive haptic device, such as the force approximation and pseudo friction cone, were investigated, and appropriate performance indices were suggested. Optimization was conducted for the 5-bar mechanism with redundant actuation, based on the proposed performance indices. Through this optimization, the maximum angles for the force approximation and pseudo friction cone were significantly decreased. A control method for selecting the activated brake was also proposed, in order to avoid unsmooth display during the wall-following task. From the various experiments, the following conclusions can be drawn:

1. The pseudo friction cone of the redundantly actuated mechanism is defined by the region situated on the opposite side of the area where the desired force is located. The passive FME of the redundantly actuated 5-bar mechanism consists of three adjacent regions and therefore eight passive FMEs are possible.
2. The optimization process allows the reference forces to be distributed more evenly, thereby enabling a displayable region to be broadened, without creating a large pseudo friction cone.
3. The motion of the end-effector along the frictionless surface requires a weaker hand force input, since the maximum force approximation angle is decreased by the optimization process.

The control action of the avoiding stick motion (i.e., the coercive force approximation) sometimes produces a poor force approximation. In the experiment, the maximum force approximation angle is observed during the control. Although the optimization can decrease the angle of force approximation, the limitation of force approximation still remains. Hence, a control method for overcoming the force approximation, such as that described in ref. 15, should be implemented. A change in the reference force can cause an abrupt change in the displayed force, so further research is required on this problem.

REFERENCES

1. J.E. Colgate, M.A. Peshkin, and W. Wannasuphoprasit, Nonholonomic haptic display, Proc IEEE Int Conf Rob Autom, Minneapolis, 1996, pp. 539–544.
2. C.H. Cho, M.S. Kim, and J.B. Song, Performance analysis of a 2-link haptic device with electric brakes, Proc 11th Symposium on Haptics, Los Angeles, 2003, pp. 47–53.
3. T. Yoshikawa, Foundations of robotics: Analysis and control, MIT Press, Cambridge, MA, 1990, pp. 127–133.
4. M.A. Peshkin, J.E. Colgate, W. Wannasuphoprasit, C.A. Moore, R.B. Gillespie, and P. Akella, Cobot architecture, IEEE Trans. Rob. Autom. 17 (2001), 377–390.
5. D. Surdilovic, R. Bernhardt, and L. Zhang, A novel class of intelligent power-assist systems based on differential CVT, Proc 11th IEEE Int Workshop Rob Human Interactive Commun, Berlin, 2002, pp. 170–175.
6. W. Book, R. Charles, H. Davis, and M. Gomes, The concept and implementation of a passive trajectory enhancing robot, Proc ASME IMECE, Dyn Syst Control Division, Atlanta, 1996, pp. 633–638.
7. J. Troccaz, S. Lavallee, and E. Hellion, PADYC: A Passive Arm with Dynamic Constraints, Proc Int Conf Adv Rob, Tokyo, 1993, pp. 166–171.
8. D.K. Swanson and W.J. Book, Obstacle avoidance methods for a passive haptic display, Proc IEEE/ASME Int Conf Adv Intell Mechatronics, Como (Italy), 2001, Vol. 2, pp. 1187–1192.
9. M. Sakaguchi, J. Furusho, and N. Takesue, Passive force display using ER brakes and its control experiments, Proc. IEEE Virtual Reality, Yokohama, 2001, pp. 7–12.
10. D. Karnopp, Computer simulation of stick-slip friction in mechanical dynamic system, ASME J. Dyn. Syst., Meas., Control 107 (1985), 100–103.
11. S. Ma, H. Yoshinada, and S. Hirose, CT ARM-I: coupled tendon-driven manipulator model I-Design and basic experiments, Proc IEEE Rob Autom, Nice, France, 1992, Vol. 3, pp. 2094–2100.
12. L. Tsai, Robot analysis: The mechanics of serial and parallel manipulators, Wiley & Sons Inc., New York, 1999, pp. 342–348.
13. Y. Nakamura, Advanced robotics: Redundancy and optimization, Addison-Wesley, Reading, MA, 1991, pp. 41–68 and 205–225.
14. S. Rao, Engineering optimization: Theory and practice, 3rd ed., Wiley & Sons Inc., New York, 1996, pp. 368–375, 502–521, and 780–781.
15. D.K. Swanson and W.J. Book, Path-following control for dissipative passive haptic displays, Proc 11th Symp Haptics, Los Angeles, 2003, pp. 101–108.